

# Machine-Learning-Based Future Received Signal Strength Prediction Using Depth Images for mmWave Communications

Hironao Okamoto, *Student Member, IEEE*, Takayuki Nishio, *Member, IEEE*,  
 Kota Nakashima, Yusuke Koda, *Student Member, IEEE*, Koji Yamamoto, *Member, IEEE*,  
 Masahiro Morikura, *Member, IEEE*, Yusuke Asai, *Member, IEEE*, and Ryo Miyatake

arXiv:1803.09698v1 [cs.NI] 26 Mar 2018

**Abstract**—This paper discusses a machine-learning (ML)-based future received signal strength (RSS) prediction scheme using depth camera images for millimeter-wave (mmWave) networks. The scheme provides the future RSS prediction of any mmWave links within the camera’s view, including links where nodes are not transmitting frames. This enables network controllers to conduct network operations before line-of-sight path blockages degrade the RSS. Using the ML techniques, the prediction scheme automatically learns the relationships between the RSS values and the time-series depth images. We apply a powerful neural-network model, which is capable of learning both spatial and long-term temporal relationships: the Convolutional Neural Network + Convolutional Long Short-Term Memory (CNN+ConvLSTM) network. We generate RSS values and depth images simulating a real-life environment using ray-tracing software and three-dimensional computer graphics (3DCG) software, and then we evaluate the accuracy of the proposed scheme and reveal the impact of camera positions on the prediction accuracy. Moreover, we conduct experiments using commercially available IEEE 802.11ad devices and an RGB-D camera to demonstrate the feasibility of the scheme in a real-life environment. Simulation and experimental results show that the CNN+ConvLSTM network achieves a higher-accuracy in future RSS value prediction compared to other ML models. Moreover, the results confirm that the scheme is feasible for real-time prediction systems and show that the scheme predicts RSS values in 0.5 s future with RMS errors of less than 2.1 dB in the simulations and 3.5 dB in the experiments.

**Index Terms**—mmWave, machine learning, link quality prediction, RGB-D camera, recurrent neural network

## I. INTRODUCTION

Millimeter-wave (mmWave) communication technology will be a key part of next-generation wireless access networks [1]–[4]. The IEEE 802.11ad standard [5] achieves multi-Gbit/s transmission rates due to the large continuous bandwidth for unlicensed use. Moreover, its high signal path loss and the highly directional antennas employed

H. Okamoto, T. Nishio, Y. Koda, K. Yamamoto, and M. Morikura are with the Graduate School of Informatics, Kyoto University, Kyoto, 606-8501 Japan (e-mail: nishio@i.kyoto-u.ac.jp).

K. Nakashima is with the Faculty of Engineering, Kyoto University, Kyoto, 606-8501 Japan.

Y. Asai and R. Miyatake are with NTT Network Innovation Laboratories, NTT Corporation, Yokosuka, Kanagawa, 239-0847 Japan.

Parts of this work were presented at the 85th IEEE Vehicular Technology Conference (VTC Spring) and the IEEE Consumer Communications and Networking Conference (CCNC).

This work was supported in part by JSPS KAKENHI Grant Number 17H03266.

in mmWave communication systems increase geographic spectrum reusability [6].

However, the characteristics of the mmWave cause a human blockage problem. Owing to highly directional antennas and their characteristics of rectilinear propagation and strong absorption by moisture and oxygen, when pedestrians block line-of-sight (LOS) paths, the received signal strength (RSS) decreases significantly [7], [8].

To solve the human blockage problem, a number of communication control schemes, such as access point (AP) handover [9], [10] and fast session transfer (FST) [11], have been considered. However, most of these schemes are reactive schemes based on current link quality, and hence the link quality sharply degrades before the control operations start as well as while the operations are ongoing. Here, link quality is determined by performance metrics such as the throughput, data transmission rates, and RSS. For example, in the handover method, a station (STA) communicating with a source AP is transferred to another AP with a better link quality when a LOS path blockage occurs. However, a search for an appropriate AP and data forwarding from the source AP to the destination AP suspended data transmission to the STA for a while [12], [13]. Therefore, it is difficult to avoid periods when link quality is significantly low. As another example, FST implemented in the IEEE 802.11ad standard provides seamless transition between 2.4/5 GHz, and 60 GHz channels. Although the transition to the 2.4/5 GHz band is effective for maintaining the wireless connection, it is difficult to maintain a constantly high link quality. This is because the throughput and data transmission rate between the AP and the STA are reduced due to its narrow bandwidth compared to the 60 GHz band.

## A. Conventional Link Quality Prediction Scheme

Link quality prediction [14] is an approach used either to avoid the link quality degradation or to shorten the link quality degradation period. The link quality prediction of any mmWave links, including links currently not communicating, provides more efficient network operations. The current link quality prediction of non-communicating links enables network controllers to detect the availability of mmWave APs, which is required to search for the destination candidate AP for the handover and to determine the channel condition of

the 60 GHz band in FST. The predicted future link quality information can further improve network throughput, quality of experience, and energy efficiency [15], [16]. The information also suppresses a handover to an AP where the link is almost blocked, which wastes the wireless resource owing to the suspension of data transmission during the handover. On the other hand, the prediction scheme should be efficient for wireless resources. This is because, for the AP search and channel condition determination, the frame transmission from every AP to the STA is commonly required to measure the link quality, and the frames are periodically transmitted to update the measured values, which can lead to consumption of bandwidth.

Previous studies [17], [18] proposed future link quality prediction schemes based on time-series prediction models. However, in mmWave communications, LOS blockage decreases link quality sharply and suddenly; therefore, link quality is not stable and the link quality degradation cannot be predicted by observing the previous link quality.

Link quality, especially RSS, can also be calculated from geometry information using ray-tracing techniques [19]–[21]. This approach predicts the future RSS independently of the previous RSS, so that it can predict the sharp and sudden RSS degradation. However, to predict future RSS, accurate moving objects detection and their movement prediction are required before these techniques can be used. In addition, the ray-tracing techniques require full 3D information, including electromagnetic characteristics of objects in the propagation environment that cannot be obtained from only images. Moreover, the techniques incur a high calculation cost in order to calculate the propagation path. According to [20], it takes more than 200 ms to simulate one frame of mmWave propagation considering two reflections with a 2 GHz CPU. Since we are mainly concerned about the RSS values when a blockage occurs, ray-tracing simulation with two reflections is required and the calculation cost becomes extremely large. In particular, for the situation where many pedestrians are in the communication area, the calculation cost of propagation paths is excessive.

#### B. Proactive Handover Based on Human Blockage Prediction

To solve the link quality degradation problem, we have proposed a camera-assisted proactive network control system for mmWave networks [22]–[25]. This system captures the geometry of an environment and the mobility of obstacles using cameras and conducts network operations such as flow control, routing, and handover proactively. This is done by considering the link quality predicted from the captured information before the blockages occurred. Moreover, this approach enables us to predict link quality without transmitting any overhead frames. In [23], we proposed a proactive handover system based on human blockage prediction using red-green-blue and depth (RGB-D) cameras. In this scheme, the network controller transfers an STA communicating with one AP to another AP before human blockage occurs and avoids throughput degradation. This proactive control is enabled by considering the captured information from the RGB-D camera.

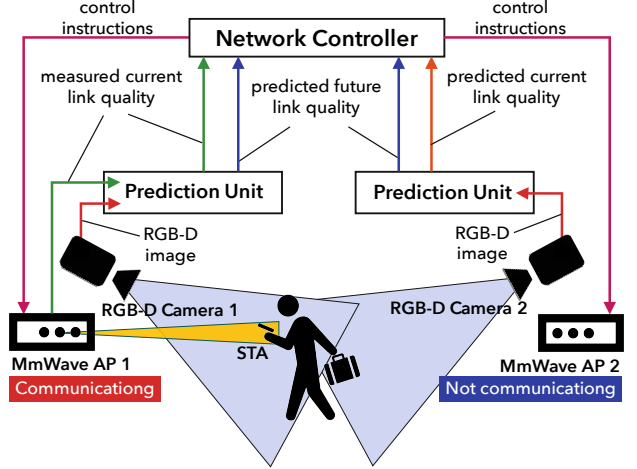


Fig. 1. Proposed system model. The prediction units predict the link quality from the RGB-D images. The network controller conducts network operations based on the predicted or measured link quality.

Using depth information from the RGB-D camera, the local wireless environment, including the locations of obstacles, can be detected. This enables an accurate prediction of current or future wireless environments [26]. The experiment confirmed that by comparing a reactive handover system [10], the system significantly reduced the amount of time when the throughput is degraded by human blockages.

Fig. 1 presents a system model using the proposed scheme. The system consists of the following components: mmWave APs, RGB-D cameras, prediction units, and a network controller. Each prediction unit is connected with the mmWave AP, RGB-D cameras, and the network controller via wired local area networks. RGB-D cameras, typified by the Microsoft Kinect [27], can capture not only color, but also depth images. These camera-to-object distance data in depth images reflect the mobility of obstacles and users, which significantly affects mmWave link quality. The cameras send the RGB-D images to the connected prediction units. Note that the prediction units may be connected to multiple cameras and can share cameras with other prediction units.

Each prediction unit receives the RGB-D images from the RGB-D cameras and predicts the current and future link quality using the images. The prediction unit sends the predicted link quality to the network controller. When the unit receives the measured link quality from the connected AP, the unit also sends it. The network controller conducts the handover based on the received measured and predicted link quality.

However, the prediction unit could not work in environments where the reflected and diffracted waves greatly influence the link quality and where objects other than pedestrians, such as a car and luggage behind the pedestrian, block the LOS path.

This is because the proactive handover scheme in [23] uses the human recognition function of Kinect to predict the future link quality. In other words, we only considered whether the LOS will be blocked or not for the predicted link quality. Hence, only pedestrian position information was utilized, and the other information, including the geometry of

the environment and position information of objects other than pedestrians, was discarded. Consequently, it cannot predict blockages due to an object other than a human body. Moreover, quantitative prediction has not been achieved yet, so that the controller cannot select an mmWave link which provides the highest link quality from a selection of LOS links. In addition, the path through which the LOS path passes within the view of the camera was required to be manually given in the study.

### C. Contribution

In this paper, we propose a machine-learning-based mmWave future RSS prediction scheme using depth images. This prediction scheme provides a more general link quality prediction as the function of the prediction unit. The scheme not only predicts the current RSS values but also future RSS values quantitatively without transmitting any frames. We use the RSS as a link quality metric because the RSS is a fundamental metric in wireless communications and is not affected by the control of upper layer protocols, such as a flow control and rate adaptation, while throughput and PHY rate are affected by these protocols. In this scheme, the network controller predicts the future RSS values from only time-series camera images by learning the relationships between RSS and time-series images with machine learning (ML) techniques [28]. Since the relationships between RSS values and time-series images are directly learned by an end-to-end ML approach, the scheme can fully utilize information underlying the images and can be adaptable to any environment. In particular, this enables the model to obtain the path through which the LOS path passes automatically and build up the ability of object recognition including objects other than a human body. Different from RSS prediction using ray-tracing techniques, the ML-based prediction works without the full 3D information of the communication area because it predicts values based on previous experience. In addition, although the ML-based prediction demands a large calculation cost to learn the prediction model, once the learning is over, it can predict the value immediately, and the calculation cost does not increase even when the number of pedestrians in the area increases.

To achieve a higher-accuracy prediction model, we used three types of ML models applicable to the prediction from time-series depth images. These employ the convolutional neural network (CNN), CNN + Convolutional Long Short-Term Memory (ConvLSTM) network, and Random Forest (RF). Then, we evaluate the RSS prediction accuracy through simulations and experiments. In addition, we also evaluate the impact of camera position on prediction accuracy through the simulations. This simulates a passage where some pedestrians pass in front of the cameras. Next, we build a testbed using commercially available IEEE 802.11ad mmWave wireless local area network (WLAN) devices and demonstrate the effectiveness of the proposed system in the real environment.

The novel contributions of this paper are the following.

- 1) Using the ML techniques, we enable the prediction scheme to automatically learn and build a model of the relationships between the RSS values and the time-series

depth images. The scheme, thereby, does not need any additional information, such as geographical information including the path through which the LOS path passes, other than RSS values and depth images. Moreover, this model enables the quantitative prediction of future RSS values, which allows a network controller to select the best mmWave link from some potential links with confidence. Such model building and RSS prediction cannot be achieved by the link quality prediction scheme in [23] because this scheme requires the path information to be given manually and is able to predict only whether the LOS will be blocked or not.

- 2) We build a novel simulation system for camera-assisted mmWave networks, and then evaluate the accuracy of our RSS prediction scheme and reveal the impact of camera positions on the prediction accuracy. This simulation system consists of a combination of a ray-tracing software and 3D computer graphics (3DCG) software, and allows us to obtain RSS values and camera images in a real-life environment by radio-wave propagation simulation and 3D animation rendering, respectively. Moreover, we show that the proposed neural network structure (CNN+ConvLSTM), which is capable of modeling complex spatiotemporal dependencies, provides the highest prediction accuracy in the prediction of future RSS values among the three ML algorithms discussed.
- 3) We also confirm that the proposed scheme works in a real-life environment through experiments. The experiments employ commercially available devices: an RGB-D camera, an IEEE 802.11ad AP, and an STA, and RSS values are measured from real IEEE 802.11ad WLAN signals. The experimental results demonstrate that the proposed scheme employing CNN+ConvLSTM realizes the real-time prediction of future RSS values.

A preliminary version of this work was presented in [24], where a machine-learning-based mmWave current throughput prediction scheme was proposed. We used throughput as link quality in that work, so that actual throughput can be affected by several factors such as a rate adaptation algorithm and offered traffic, and therefore, it was difficult to predict the current throughput values only from the images. Moreover, the preliminary work was limited to the prediction of the current throughput values and prediction of future throughput value was not considered. Another preliminary version of this work was presented in [25], where we evaluated the accuracy only in a simulation of current RSS value prediction using more simple ML models and one camera position.

This paper is organized as follows. Section II describes the ML-based RSS prediction system and its operation. Section III introduces the ML algorithms and presents the proposed ML architectures. Section IV shows the simulation results and discusses the accuracy of each ML algorithm and camera position. Section V demonstrates the experimental results and discusses the accuracy of the prediction. Finally, conclusions are presented in Section VI.

## II. MACHINE-LEARNING-BASED RSS PREDICTION

### A. System model

The system model of the proposed scheme is consistent with the previous work described in Section I-B. Unlike [23], the prediction units not only predict whether the LOS will be blocked but also learn the relationships between the measured RSS values and images and predict the RSS values from the images.

Each prediction unit performs the two different operations depending on the availability of the measured RSS. First, when the prediction unit receives the measured RSS from the connected AP, the prediction unit performs a learning and prediction operation. In this situation, the prediction unit learns the relationships between the RSS and the time-series RGB-D images. Then, the prediction unit predicts the future RSS using the time-series RGB-D images and sends the prediction results to the network controller. The measured RSS is also forwarded to the network controller.

Second, when the prediction unit does not receive the measured RSS, the prediction unit performs a prediction operation. The prediction unit predicts the current and future RSS values using the time-series RGB-D images based on the model learned in the previous operation. Then, the prediction unit sends them to the network controller. The network controller conducts the handover based on the measured and predicted RSS values received from the prediction units.

In this paper, we assume that STAs are static. It is considered that the position of the STA can also be tracked from the camera images using localization techniques like [26]. However, our purpose is to show that the relationships between the RSS values and the depth images can be modeled using ML techniques, and therefore, the tracking of the STA is out of the scope of this paper. Depth information can be obtained not only from one RGB-D camera but also two or more RGB cameras using stereo vision techniques [29]. RGB cameras are widely available as surveillance cameras in crowded places such as railway stations and commercial facilities. These are primary targets for mmWave communications deployment; therefore, it may not be necessary to deploy RGB-D cameras for this prediction scheme.

### B. Dataset Generation

Fig. 2 shows the dataset generation procedure. In the learning operation, the RGB-D camera captured depth images at 30 fps, and the AP simultaneously captured the RSS values of the STA. The prediction unit generated a training dataset from these captured images and RSS values.

Let  $y_t$  be the measured RSS value obtained from an mmWave AP and  $i_t$  be the depth image obtained from a RGB-D camera at time  $t$ . Firstly, the resolution of each image was reduced to  $40 \times 40$  (height  $\times$  width) in order to decrease calculation complexity. Let  $i'_t$  be the reduced depth image. Then, 16 consecutive images, which are images obtained in 0.53 s, were combined as an image sequence, which was used as an input of the ML algorithms  $x_t = \{i'_{t-15}, i'_{t-14}, i'_{t-13}, \dots, i'_t\}$ . By using the images for 0.53 s, the fluctuation of walking speed induced by the walking motion of a human being, which is

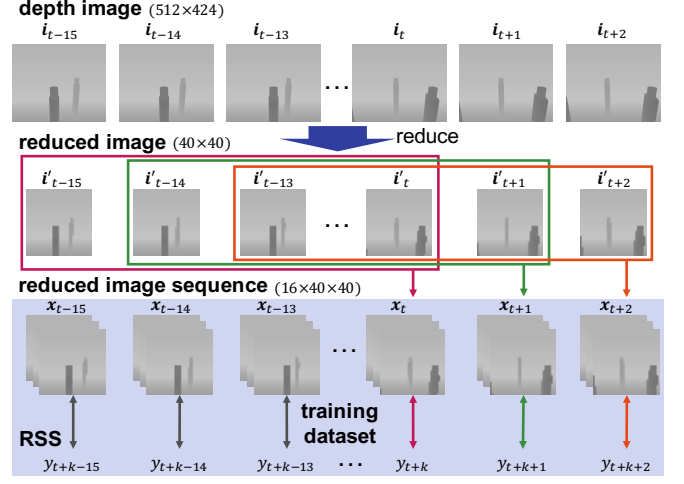


Fig. 2. The dataset generation procedure. The depth images were reduced, combined, and associated with the future RSS values before training. The RSS values in  $k$  frames after will be predicted.

around 2 Hz [30], was expected to be averaged out, and that results in accurate prediction of human movement. In order to predict the future RSS values, the image sequences were associated with the future RSS values. Therefore, for example, to predict the RSS values in  $k$  frames (equal to  $k/30$  s),  $x_t$  was associated with  $y_{t+k}$ .

## III. MACHINE LEARNING ALGORITHMS AND MODEL

This section introduces the ML algorithms employed by our RSS prediction scheme and presents our proposed ML models.

### A. Machine Learning Algorithm

1) *Convolutional Neural Network*: The Convolutional Neural Network (CNN), which employs convolutional layers, is one of the most successful deep learning models. It has achieved a competitive performance in many visual tasks [31]. In 2D CNN, convolutions are applied on 2D images. These extract features implied in spatial information. Furthermore, the 3D CNN extracts features from both spatial and temporal dimensions.

2) *Convolutional LSTM*: The Long Short-Term Memory (LSTM) network [32] is a widely used recurrent neural network (RNN) architecture. RNN can model the time-dependent relationships among inputs and outputs. Hence, it has been employed for sequential modeling and prediction problems in wireless communications and computer vision [33]–[35]. The Convolutional LSTM (ConvLSTM) network [36] is an extension of the LSTM architecture, which has convolutional structures and enables us to handle not only spatial but also temporal sequence prediction problems. It is expected that the ConvLSTM network learns longer-term spatiotemporal features than the 3D CNN.

The ConvLSTM layer calculates its output and learns the model from past output and input according to the following procedure. Let  $X_t$  be an input vector,  $H_t$  be an output vector,  $C_t$  be cell outputs, and  $i_t, f_t, o_t$  be outputs of input, forget,

and output gate of the ConvLSTM layer, respectively, at time  $t$ . These are all 3D tensors whose last two dimensions are spatial dimensions (rows and columns). The ConvLSTM calculates outputs using the following equations:

$$i_t = \sigma(W_i * X_t + U_i * H_{t-1} + b_i), \quad (1)$$

$$f_t = \sigma(W_f * X_t + U_f * H_{t-1} + b_f), \quad (2)$$

$$o_t = \sigma(W_o * X_t + U_o * H_{t-1} + b_o), \quad (3)$$

$$C_t = f_t \odot C_{t-1} + i_t \odot \tanh(W_c * X_t + U_c * H_{t-1} + b_c), \quad (4)$$

$$H_t = o_t \odot \tanh(C_t), \quad (5)$$

where  $\sigma(\cdot)$  is the sigmoid function  $\sigma(x) = 1/(1 + \exp(-x))$ ,  $*$  denotes the convolution operator, and  $\odot$  represents a Hadamard product, which is also called a pointwise product.  $W_\diamond$  and  $U_\diamond$  are two dimensional convolutional kernels and  $b_\diamond$  are biases, where  $\diamond$  denotes  $i$ ,  $f$ ,  $o$  and  $c$ . These are parameters of the ConvLSTM that should be learned through training.

3) *Random Forest*: Random Forest (RF) [37] is one of the most typical ensemble learning models. A well-known application of this model is 3D location prediction of individual body parts using an RGB-D image [38]. RF consists of many simple decision trees using a bootstrap sample of the data and a randomly selected subset of input features at each split while growing each tree. Every tree predicts its output from an input vector, and the model outputs the mean prediction of these outputs. Thus, RF has the advantage of two ML algorithms; bagging [39] and random variable selection. This leads to a stable and accurate model.

### B. Proposed Machine Learning Models

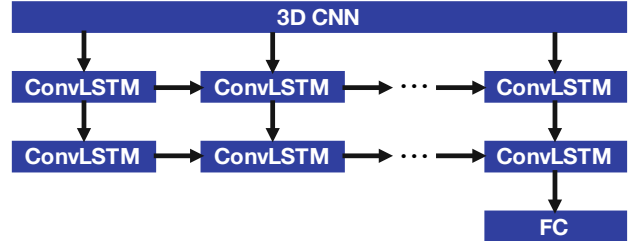
We employed three types of ML models: CNN+ConvLSTM network, CNN network, and RF. Fig. 3 presents the structures of the NNs. These NNs take a three-dimensional input  $x_t$  and return an RSS value  $y_{t+k}$ . They consist of several layers: 3D convolution (3D Conv), ConvLSTM, Fully Connected (FC), and an average pooling layer. Each layer gets its input from the previous layer and feeds its output to the next layer. Moreover, we employ Batch Normalization (BN), Rectified Linear Unit (ReLU) activation, and a Flattening operation.

The average pooling layer reduces the size of feature maps by averaging the values that reduce calculation cost. BN [40] allows us to use much higher learning rates and be less careful about initialization in order to accelerate training. ReLU is the most widely used activation function. It is used to gain the non-linearity of the network. The FC layers are used to predict the RSS values from the feature map output from the previous layer.

The first two 3D Conv layers adopt 64 and 128 convolution kernels of size  $3 \times 3 \times 3$  (time  $\times$  height  $\times$  width). These 3D Conv layers are utilized to extract spatial features of each depth image. The ConvLSTM layers adopt 64 convolution kernels of size  $3 \times 3$  (height  $\times$  width). The first ConvLSTM layer returns 3D feature maps, while the second ConvLSTM layer returns 2D maps as shown in Fig. 3(b). In the CNN, we employ three 3D Conv layers which have 64 kernels of size  $3 \times 3 \times 3$ ,  $3 \times 3 \times 3$ , and  $8 \times 1 \times 1$ , in order. This is instead of



(a) The overview of our NNs. The two ConvLSTM layers in the CNN+ConvLSTM Network are replaced for convolution layers in the CNN.



(b) The structure of ConvLSTM layers in the CNN+ConvLSTM network. The first ConvLSTM layer returns spatiotemporal feature maps, while the second ConvLSTM layer returns spatial maps.

Fig. 3. The structures of our NNs.

the preceding ConvLSTM layers where the final output size of these three convolution layers is consistent with that of the two ConvLSTM layers. While these two ConvLSTM layers or three 3D Conv layers are utilized to extract temporal features of each depth image, it is expected that the ConvLSTM layers can extract longer-term temporal features than the 3D Conv layers. BN and a ReLU activation are applied after every ConvLSTM and 3D Conv layer, except a fourth 3D Conv layer in the CNN. The pool size of the average pooling layer is  $2 \times 2 \times 2$ . This means each dimensional size of the feature map is reduced by half. Then, the spatial feature maps are reduced to one-dimensional feature vectors in the flattening operation and the vectors are fed to the FC layers. The unit

TABLE I  
PARAMETERS OF THE ML ALGORITHMS.

ML algorithm	Parameter	Value
CNN & CNN+ConvLSTM	batch size	64
	epochs	200
	loss function	mean squared error
RF	number of trees	20
	maximum depth of the tree	20
	splitting criterion	mean squared error

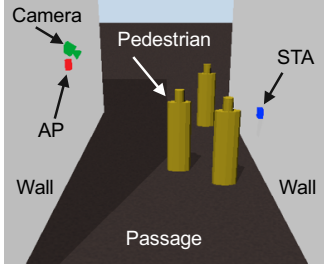


Fig. 4. 3D spatial model. The camera is placed at position  $A_{low}$  in Fig. 5.

number of the two FC layers are 512 and 1, in order, and the first FC layer is followed by ReLU activation.

We optimized the NNs using Nadam [41] with an initial learning rate of 0.001 and the other arguments set by default values. The learning rate is dropped to its 0.975 every iteration. We split the training data into training and test sets with a ratio of 80% and 20% respectively. When training NNs, we use 25% of the training set as a holdout validation set. A GeForce GTX 1080 Ti GPU is used to train each network.

RF can only take one-dimensional inputs, so a three-dimensional input  $x_t$  is reduced to one-dimensional feature vectors before the input is fed to the RF algorithm. The other parameters of the ML algorithms are shown in TABLE I. We used Keras [42] with TensorFlow [43] backend and scikit-learn [44] for the implementation of the NNs and RF, respectively.

#### IV. SIMULATION EVALUATION

We performed simulations to evaluate the RSS prediction accuracy of each ML algorithm. Through these simulations, we generate many data sets of situations where we place a camera in multiple places and evaluate the impact of camera position on prediction accuracy.

##### A. Simulation Setup

We first generated a 3D spatial model of the mmWave communication area. Then, using the 3D spatial model and mmWave propagation model, the RSS values were calculated using a radio propagation simulator. Simultaneously, using the 3D spatial model and 3DCG techniques, camera images were captured by a 3DCG modeler. Using this generated dataset of the RSS values and images, we evaluated the prediction accuracy of each algorithm.

In this simulation, we considered the 3D passage model with a point-to-point mmWave communication system presented in Figs. 4 and 5. The length and width of the passage were 10 m

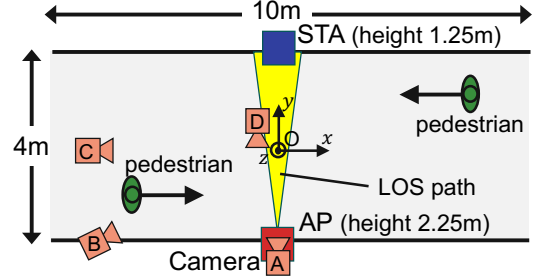


Fig. 5. Passage model. The width of the passage is 4 m and the length is 10 m. Pedestrians walk on the right-hand side of the passage, from their perspective. A camera is placed at one of the eight positions: A–D in the X-Y plane and at a height of 2.25 m (low) or 5 m (high).

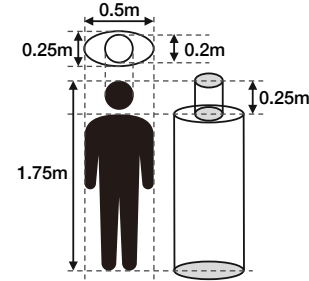


Fig. 6. Human model. We use a twin cylinder model [45] as the human shape model.

and 4 m, respectively, and the height of the walls was 10 m. An AP, an STA, and a camera were present in the passage. Letting the center of the passage be the coordinate origin O, the AP was placed at  $(x, y, z) = (0, -2, 2.25)$  and the STA was placed at  $(0, 2, 1.25)$ . The units of the x, y, and z axes were meters. We considered that the AP and STA were constantly communicating with each other using a radio frequency of 60 GHz. The AP antenna was a directional antenna with a 15-degree beam width and 24 dBi gain at 60 GHz. The antenna was facing toward the STA and the transmission power was 100 mW. The STA antenna was an omnidirectional antenna and the minimum sensitivity was set to  $-68$  dBm, which is the required sensitivity for the lowest PHY rate for data transmission in IEEE 802.11ad [5]. We assume that frames with RSS values of less than  $-68$  dBm will fail to receive and RSS value of less than  $-68$  dBm can not be measured. In order to simply simulate it, RSS value of less than  $-68$  dBm was rounded to  $-68$  dBm in the simulations. The camera was placed at one of the eight positions shown in Fig. 5. The simulation ran for 30 min, and therefore, the dataset had 54000 pairs of the RSS values and images.

The pedestrians came in from either side of the passage and walked straight, as shown in Fig. 5, with speeds in the range of  $[0.5, 2]$  m/s. The y-directional positions of the pedestrians who walked from the left side to the right side were distributed uniformly in the range  $[-1.75, 0]$  m and those of pedestrians who walked from the right side to the left side were distributed uniformly in the range  $[0, 1.75]$  m. We set pedestrians entering the passage to follow a Poisson distribution as per [46]. Since we were primarily concerned with the situation only when

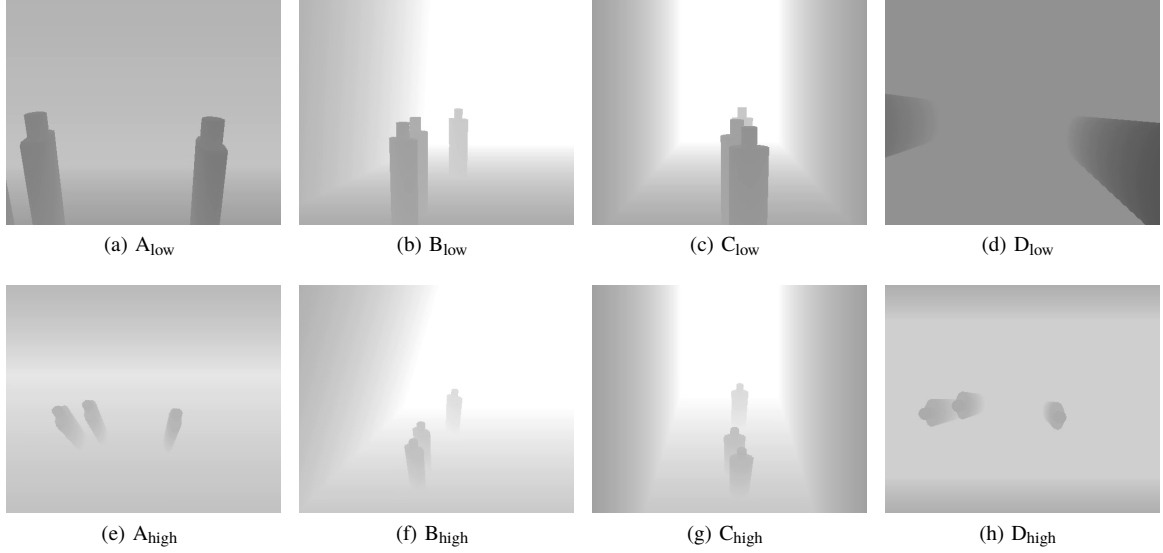


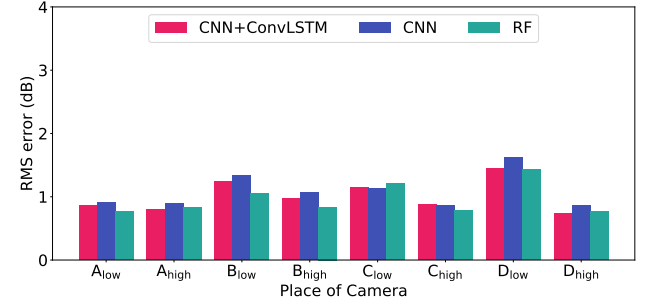
Fig. 7. A camera image is generated at each camera position. The camera positions are referred to in Fig. 5.

some pedestrians block the LOS path simultaneously, we considered Poisson arrivals to be an adequate scenario for our study. We set the parameter of the Poisson distribution to  $\lambda = 0.25$ .

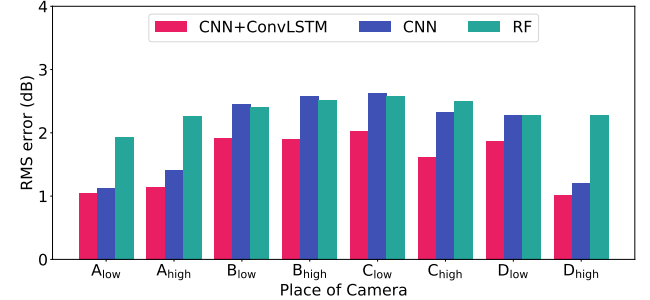
The shape of a pedestrian was modeled by a twin cylinder model [45], as shown in Fig. 6. This is a model for a calculation of the human body shadowing in the mmWave communications. The magnetic permeability and electric constants of human bodies were assumed to be the same values as those of water. This provided shadowing properties similar to those of real humans [47]. We calculated the RSS values using the radio propagation simulator RapLab [48], which conducts 3D ray tracing using imaging methods.

We employed a depth camera equivalent to the Kinect v2, which has a resolution of  $512 \times 424$  pixels, an angular field of view of  $60^\circ$  in the vertical plane,  $70^\circ$  in the horizontal plane, and a depth capture range of 0.5–8 m. We considered eight patterns for the camera position of A: (0, -2), B: (-4, -2), C: (-4, 0), or D: (0, 0) in the X-Y plane and a height of 2.25 m (low) or 5 m (high). This was in order to evaluate the accuracy of the proposed prediction scheme with respect to camera position. The camera at each position was pointed at (0, 0, 1.75), which was the midpoint between the AP and the STA. We generated the depth images using the 3DCG modeler Blender [49]. The images from various camera positions are shown in Fig. 7.

The algorithms predicted an RSS value in 0 s (current) or 0.5 s (future) after. Therefore,  $k$  was set to 0 and 15, respectively. In the channel model for 60 GHz WLAN systems [50], the duration of the signal level degradation is characterized by a Weibull distribution with the shape parameter  $\alpha = 6.32$  and the scale parameter  $\beta = 0.59$ . Hence, the average duration of the degradation is 0.55 s, so that if we predicted an RSS value in 0.5 s, we could get most of the RSS time variation during the blockage.



(a) RMS error when the RSS values in 0 s are predicted. That is, the error of a current RSS prediction for each algorithm.



(b) RMS error when the RSS values in 0.5 s are predicted. That is, the error of a future RSS prediction for each algorithm.

Fig. 8. RMS error of each algorithm.

### B. Simulation Results and Evaluation

Fig. 8 shows the RMS error of each simulation of the camera position. Fig. 9 presents the time series of the simulated RSS values and the RSS values predicted by each algorithm when the camera was placed at position A<sub>low</sub>, A<sub>high</sub>, C<sub>low</sub>, and C<sub>high</sub>.

Figs. 8 and 9 show that each prediction method accurately predicted the current RSS values but only from depth images. On the other hand, they also show that the RF-based method has a low prediction accuracy for the future RSS value in 0.5 s at every camera position. It is considered that the RF-

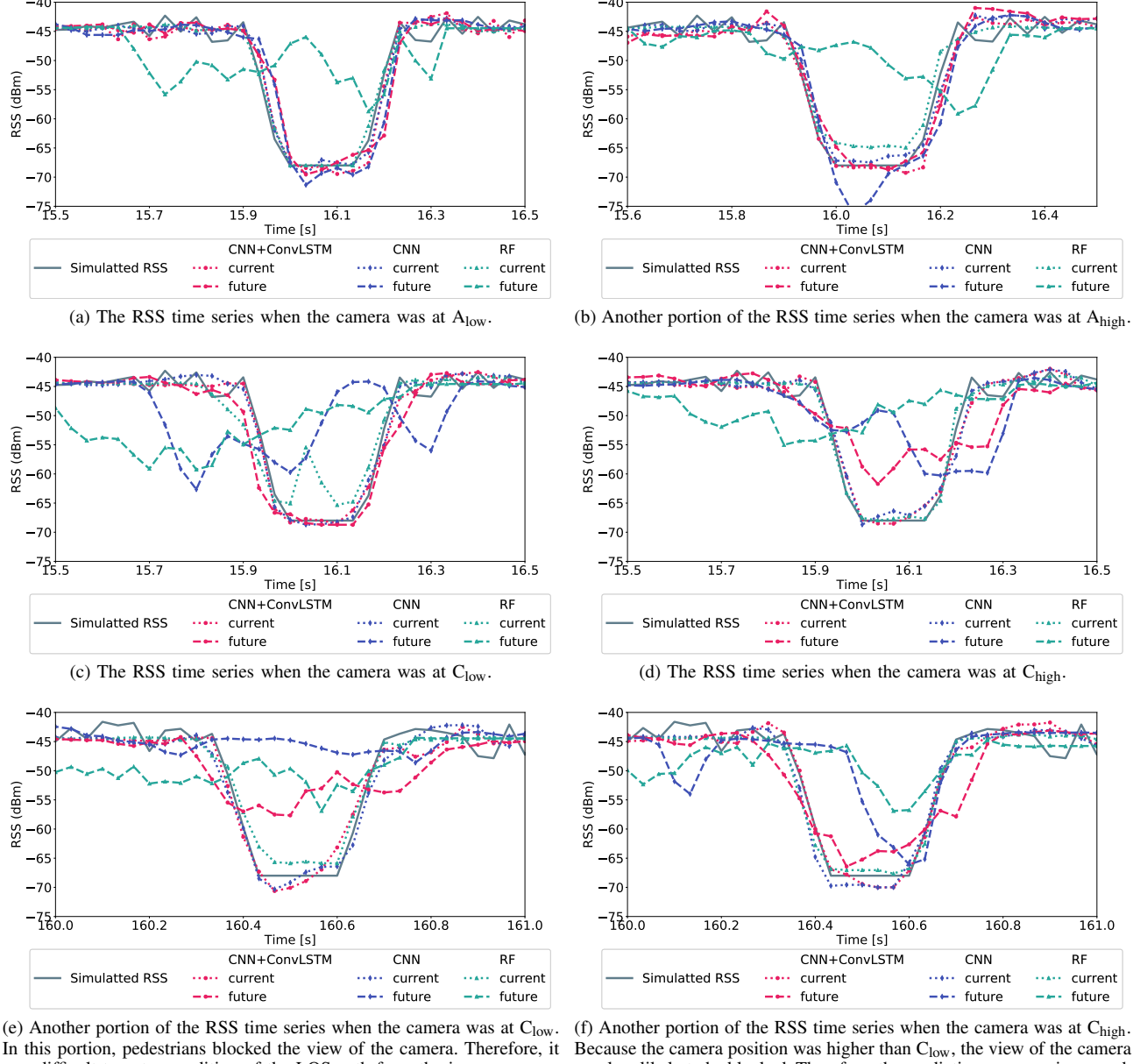


Fig. 9. Portions of the simulated and predicted RSS time series.

based method cannot predict the future RSS values because it has less ability to model the time-dependent relationships. In addition, the CNN-based method could predict a future RSS degradation when the camera was at  $A_{\diamond}$  or  $D_{\diamond}$ . It could not predict the future RSS values when the camera was at  $B_{\diamond}$  or  $C_{\diamond}$ , where  $\diamond$  denotes high and low. This is because when the camera was placed at  $B_{\diamond}$  or  $C_{\diamond}$  it was difficult to predict the movement of a pedestrian accurately compared to when the camera was placed at  $A_{\diamond}$ . When the camera was placed at  $A_{\diamond}$  or  $D_{\diamond}$ , LOS blockages could be detected easily by determining whether or not pedestrians were present in the pixels associated with the LOS path. However, when the camera was placed at  $B_{\diamond}$  or  $C_{\diamond}$ , the LOS blockage depended not only on the presence of pedestrians but also on whether

or not the depth values of the pixels fell within a certain range. In particular, the pixel values in a reduced image are averaged through the reduction process and there could be a large divergence from the actual depth value for some pixels. This leads to the misestimation of the pedestrians' positions. We consider that the CNN+ConvLSTM-based method can compensate for this error due to its ability to model long-term time dependencies. Therefore, it can better predict the future RSS values than other algorithms even when the camera is at  $B_{\diamond}$  or  $C_{\diamond}$ .

When some pedestrians were in the passage, the algorithms seemed to be unable to learn proper models and predict accurate RSS values as shown in Fig. 9(e). This is because when the camera was placed at  $B_{\diamond}$  or  $C_{\diamond}$ , the camera view was

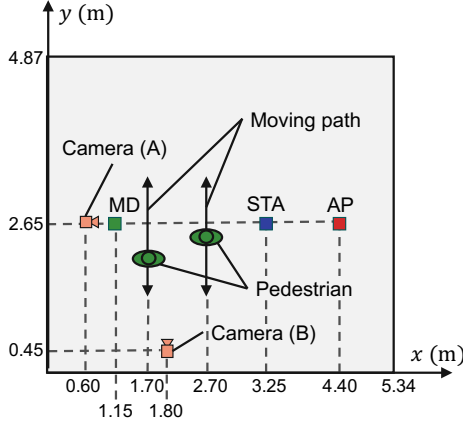


Fig. 10. Top view of the experimental environment. The measurement device (MD) captures the RSS values of the signals transmitted from the AP to the STA.

sometimes blocked by pedestrians, like in Figs. 7(b) and 7(c). Therefore, the camera could not capture the condition behind the pedestrians. When the camera was placed at  $A_{\circ}$ , the camera view could also be blocked by pedestrians. However, when the LOS path was blocked from the view of the camera, the LOS path of the mmWave was also simultaneously blocked. Hence, the NNs could accurately predict the RSS values even when the view of the camera was being blocked at camera position  $A_{\circ}$ .

Higher camera positions made the camera view less likely to be blocked by pedestrians and could prevent the degradation of the RSS prediction accuracy caused by blockages of the camera view as shown in Figs. 9(e) and 9(f). On the other hand, the higher camera positions made the pedestrians smaller in the images and made it more difficult to predict the movement of the pedestrians. Hence, the higher camera positions could degrade the prediction accuracy, as shown in Figs. 9(c) and 9(d). This was especially true when a few pedestrians were in the passage and prediction accuracy was already high for a lower camera position.

In future RSS value predictions, the camera position at  $A_{\circ}$  and  $D_{\text{high}}$  enabled the most-accurate prediction of the RSS values for every algorithm. Although the prediction accuracy was likely to be high even when the camera position was at  $D_{\text{low}}$ , the camera at  $D_{\text{low}}$  was too low to capture the whole LOS path which led to a low prediction accuracy. These results suggest that a camera position over the AP or the position overlooking the passage provided a higher prediction accuracy.

The average computation time for predicting an RSS value from time-series images using the CNN+ConvLSTM, 3D CNN, and RF schemes was about 2.9 ms, 2.1 ms and 0.20 ms, respectively. These periods were sufficiently shorter than the interval of image acquisition, and thus, it is expected that the proposed prediction schemes work in a real-time basis.



Fig. 11. Generated camera image at each camera position. The camera positions are referred to in Fig. 10.

TABLE II  
EXPERIMENTAL EQUIPMENT.

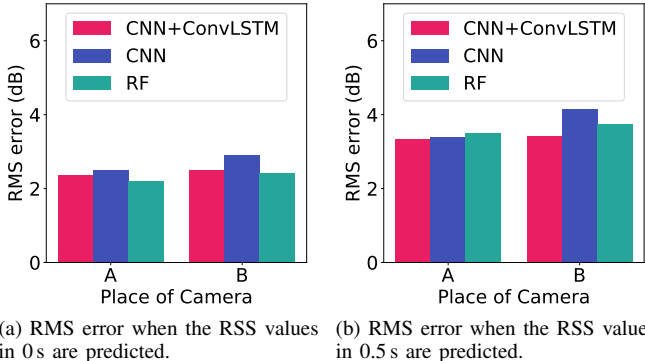
IEEE 802.11ad WLAN AP	Dell Wireless Dock D5000
IEEE 802.11ad WLAN STA	Dell Latitude E5540
Measurement device antenna	Horn antenna, 24 dBi
RGB-D camera	Microsoft Kinect for Windows (Model:1656)

## V. EXPERIMENTAL EVALUATION

### A. Experimental Setup

We also performed experiments to confirm the feasibility of the prediction schemes in a real environment. We first captured the RSS values and depth images, and then we learned the relationships between them using part of the captured data and tested the performance of the learned model using the rest of the data. To measure a time-varying RSS of IEEE 802.11ad WLAN signals in the 60 GHz band, we developed an RSS measurement system proposed in a previous work [51]. The system consisted of an AP, an STA, a measurement device (MD) and an RGB-D camera as shown in Fig. 10. The heights of the AP, the STA, and the MD were 0.70 m, 0.65 m, and 0.85 m, respectively. The camera was placed in either position A or B in Fig. 10, and images from the camera positions are shown in Fig. 11. The height of position A was 1.50 m and that of B was 1.25 m. Details of the experimental equipment are provided in TABLE II. The AP, the STA, and the RGB-D camera were all commercial products.

In the experiments, we fixed the direction of the communication link and ignored beamforming effects on the measured RSS values in order to improve the reproducibility of the experiments. This was because the implementation of beamforming operations on mmWave devices depends on many factors such as antenna parameters and beamforming algorithms. In addition, our purpose was not to show that the proposed scheme can learn the relationships between beamforming operations and RSS values. In the experiments, the MD was located behind the STA, and two pedestrians traveled between the STA and the MD moving along the path shown in Fig. 10. This allowed us to fix the beam direction of the AP antenna, because the measured RSS values at the MD were not affected by the beamforming control even when the LOS path between the STA and MD was blocked. That is, the MD was regarded as a practical STA in the experiments. The MD captured the 60.48 GHz signal and converted it to



(a) RMS error when the RSS values in 0s are predicted. (b) RMS error when the RSS values in 0.5s are predicted.

Fig. 12. RMS error of each algorithm.

an intermediate-frequency (IF) at 2.98 GHz. Then, a spectrum analyzer, equipped with the MD, measured the power of the IF signal. We treated this measured signal power as the RSS at the MD. Although the measurement was limited by the noise floor of the spectrum analyzer, the RSS values greater than approximately  $-40$  dB could be measured.

Each pedestrian moved with a random speed and blocked the LOS path almost every 6 s. The experiment ran for approximately 10 min and models were trained for 100 epochs. The other parameters were the same as for the simulation.

### B. Experimental Results and Evaluation

Fig. 12 presents the RMS error of each simulation. Fig. 13 presents the time series of the measured RSS values, as well as the RSS values predicted by each algorithm when the camera was placed at positions A or B.

The RSS prediction values in the future prediction largely match the actual values; however, the timings when the predicted values drop were sometimes shifted by several frames from the actual values as shown in Fig. 13(f). This is because the walking speed of a pedestrian varies with time in the real environment. In particular, it is difficult to obtain a change in the walking speed of the pedestrians behind other pedestrians. Hence, the blockage of the camera's view results in a possibly erroneous prediction of the LOS blockage timing. It can be addressed by placing the camera at a somewhat higher position as described in Section IV-B.

In the prediction of current values, the RF-based method more accurately predicted the current RSS value. This is because the values predicted by the CNN+ConvLSTM-based method fluctuate due to overfitting the time variation of the measured RSS values in LOS communication. The RF-based method does not fluctuate. Although NNs tends to over fit due to their high flexibility, RF with a bagging strategy can avoid overfitting.

By contrast, in the prediction of future values, the RF-based method could not predict RSS attenuation well and resulted in larger RMS errors than the CNN+ConvLSTM-based method even though it avoided fluctuations in LOS communication. This is because RF has less ability to model the time-dependent relationships.

These results suggest that the RF-based method provides a sufficiently high accuracy in the prediction of current RSS

values. However, the CNN+ConvLSTM-based method should be used in future predictions. Moreover, these results show that our ML-based RSS prediction method can predict most future RSS degradations even for a prediction in 0.5 s. In addition, the average computation time for predicting an RSS value using the CNN+ConvLSTM, 3D CNN, and RF schemes was about 3.0 ms, 3.0 ms, and 0.07 ms, respectively, which confirmed that the prediction method works in real-time.

## VI. CONCLUSION

We proposed a machine-learning-based future RSS prediction scheme using depth images. Specifically, the relationships between time-series depth images and future RSS values were learned, and then the future RSS values were predicted only from time-series depth images. The ML techniques allowed the scheme to learn the prediction model automatically and enabled the future RSS prediction from only the images. We constructed a prediction model employing three ML algorithms: CNN, CNN+ConvLSTM, and RF, and evaluated their prediction accuracy through simulations and experiments, where we predicted the RSS values at a current time and for 0.5 s ahead from the time-series depth images. We have presented various simulation and experimental results to show the prediction accuracy of the proposed scheme. These results show that CNN+ConvLSTM achieved the highest accuracy in the future RSS value prediction, where it predicted RSS values for 0.5 s ahead with RMS errors of less than 2.1 dB in the simulations and 3.5 dB in the experiments. In addition, the results revealed the impact of camera position and the surrounding conditions on prediction accuracy. Furthermore, our experimental results confirmed that the prediction scheme predicted most of the future RSS degradations even for a prediction of 0.5 s ahead in a real-life environment and that it operated fast enough for real-time use.

## REFERENCES

- [1] C. Dehos, J. González, A. De Domenico, D. Kténas, and L. Dussupt, "Millimeter-wave access and backhauling: The solution to the exponential data traffic increase in 5G mobile communications systems?" *IEEE Commun. Mag.*, vol. 52, no. 9, pp. 88–95, Sep. 2014.
- [2] P. Wang, Y. Li, L. Song, and B. Vučetić, "Multi-gigabit millimeter wave wireless communications for 5G: From fixed access to cellular networks," *IEEE Commun. Mag.*, vol. 53, no. 1, pp. 168–178, Jan. 2015.
- [3] IEEE P802.11 Task Group ay, <https://mentor.ieee.org/802.11/dcn/14/11-14-1151-08-ng60-ng60-proposed-par.docx>.
- [4] K. Sakaguchi, G. K. Tran, H. Shimodaira, S. Nanba, T. Sakurai, K. Takinami, I. Siaud, E. C. Strinati, A. Capone, I. Karls, R. Arai, and T. Haustein, "Millimeter-wave evolution for 5G cellular networks," *IEICE Trans. Commun.*, vol. 98, no. 3, pp. 388–402, Mar. 2015.
- [5] "Wireless LAN Medium Access Control (MAC) and Physical Layer (PHY) Specifications Amendment 3: Enhancements for Very High Throughput in the 60 GHz Band," IEEE Std. 802.11ad, IEEE 802.11 Working Group, 2012.
- [6] T. S. Rappaport, S. Sun, R. Mayzus, H. Zhao, Y. Azar, K. Wang, G. N. Wong, J. K. Schulz, M. Samimi, and F. Gutierrez, "Millimeter wave mobile communications for 5G cellular: It will work!" *IEEE Access*, vol. 1, pp. 335–349, May 2013.
- [7] S. Collonge, G. Zaharia, and G. E. Zein, "Influence of the human activity on wide-band characteristics of the 60 GHz indoor radio channel," *IEEE Trans. Wireless Commun.*, vol. 3, no. 6, pp. 2396–2406, Nov. 2004.
- [8] K. Haneda, "Channel models and beamforming at millimeter-wave frequency bands," *IEICE Trans. Commun.*, vol. 98, no. 5, pp. 755–772, May 2015.

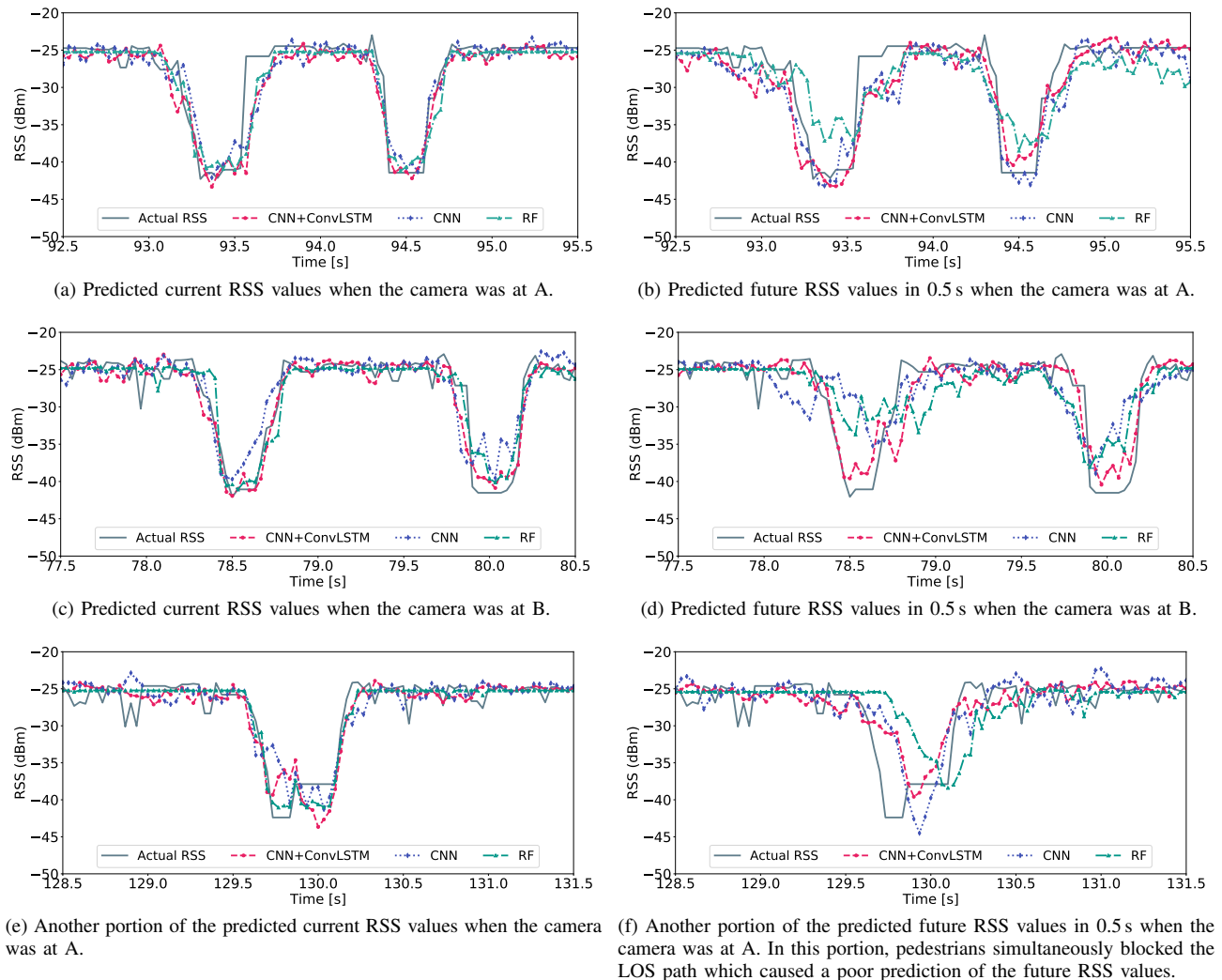


Fig. 13. Portions of the measured and predicted RSS time series.

- [9] B. Gao, Z. Xiao, C. Zhang, L. Su, D. Jin, and L. Zeng, "Double-link beam tracking against human blockage and device mobility for 60-GHz WLAN," in *Proc. IEEE WCNC*, Istanbul, Turkey, Apr. 2014, pp. 323–328.
- [10] Y. M. Tsang and A. S. Y. Poon, "Detecting human blockage and device movement in mmWave communication system," in *Proc. IEEE GLOBECOM*, Houston, Texas, USA, Dec. 2011, pp. 1–6.
- [11] E. Perahia and M. X. Gong, "Gigabit wireless lans: an overview of ieee 802.11 ac and 802.11 ad," *ACM SIGMOBILE Mobile Computing and Communications Review*, vol. 15, no. 3, pp. 23–33, Jul. 2011.
- [12] C. N. Barati, S. A. Hosseini, S. Rangan, P. Liu, T. Korakis, S. S. Panwar, and T. S. Rappaport, "Directional cell discovery in millimeter wave cellular networks," *IEEE Trans. Wireless Commun.*, vol. 14, no. 12, pp. 6664–6678, Dec. 2015.
- [13] M. Polese, M. Giordani, M. Mezzavilla, S. Rangan, and M. Zorzi, "Improved handover through dual connectivity in 5G mmwave mobile networks," *IEEE J. Sel. Areas Commun.*, vol. 35, no. 9, pp. 2069–2084, Sep. 2017.
- [14] N. Baccour, A. Koubâa, L. Mottola, M. A. Zúñiga, H. Youssef, C. A. Boano, and M. Alves, "Radio link quality estimation in wireless sensor networks: A survey," *ACM Trans. Sen. Netw.*, vol. 8, no. 4, pp. 34:1–34:33, Sep. 2012.
- [15] H. Abou-zeid, H. S. Hassanein, and S. Valentin, "Optimal predictive resource allocation: Exploiting mobility patterns and radio maps," in *Proc. IEEE GLOBECOM*, Atlanta, GA, USA, Dec. 2013, pp. 4877–4882.
- [16] H. Abou-zeid, H. S. Hassanein, and R. Atawia, "Towards mobility-aware predictive radio access: modeling; simulation; and evaluation in LTE networks," in *Proc. ACM MSWiM*. Montreal, Canada: ACM, Sep. 2014, pp. 109–116.
- [17] L. Liu, Y. Fan, J. Shu, and K. Yu, "A link quality prediction mechanism for WSNs based on time series model," in *Proc. IEEE UIC/ATC*, Xi'an, Shaanxi, China, Oct. 2010, pp. 175–179.
- [18] K. Farkas, T. Hossmann, F. Legendre, B. Plattner, and S. K. Das, "Link quality prediction in mesh networks," *Comput. Commun.*, vol. 31, no. 8, pp. 1497–1512, May 2008.
- [19] M. Jacob, S. Priebe, A. Maltsev, A. Lomayev, V. Erceg, and T. KÄijrner, "A ray tracing based stochastic human blockage model for the IEEE 802.11ad 60 GHz channel model," in *Proc. IEEE EUCAP*, Rome, Italy, Apr. 2011, pp. 3084–3088.
- [20] V. Degli-Esposti, F. Fuschini, E. M. Vitucci, M. Barbiroli, M. Zoli, L. Tian, X. Yin, D. A. Dupleich, R. MÄijller, C. Schneider, and R. S. ThomÄd, "Ray-tracing-based mm-wave beamforming assessment," *IEEE Access*, vol. 2, pp. 1314–1325, Oct. 2014.
- [21] G. R. MacCartney, S. Deng, S. Sun, and T. S. Rappaport, "Millimeter-Wave human blockage at 73 GHz with a simple Double Knife-Edge diffraction model and extension for directional antennas," in *Proc. IEEE VTC-Fall*, Montreal, Canada, 2016, pp. 1–6.
- [22] T. Nishio, R. Arai, K. Yamamoto, and M. Morikura, "Proactive traffic control based on human blockage using RGB-D cameras for millimeter-wave communications," in *Proc. IEEE CCNC*, Las Vegas, Nevada, USA, Jan. 2015, pp. 23–24.
- [23] Y. Oguma, T. Nishio, K. Yamamoto, and M. Morikura, "Proactive handover based on human blockage prediction using RGB-D cameras for mmWave communications," *IEICE Trans. Commun.*, vol. 99, no. 8, pp. 1734–1744, Oct. 2016.

[24] H. Okamoto, T. Nishio, M. Morikura, K. Yamamoto, D. Murayama, and K. Nakahira, "Machine-learning-based throughput estimation using images for mmWave communications," in *Proc. IEEE VTC 2017-Spring*, Sydney, Australia, Jun. 2017, pp. 1–6.

[25] H. Okamoto, T. Nishio, M. Morikura, and K. Yamamoto, "Recurrent neural network-based received signal strength estimation using depth images for mmwave communications," in *Proc. IEEE CCNC*, Las Vegas, Nevada, USA, Jan. 2018, pp. 1–2.

[26] J. Biswas and M. Veloso, "Depth camera based indoor mobile robot localization and navigation," in *Proc. IEEE ICRA*, St Paul, MN, USA, May 2012, pp. 1697–1702.

[27] Kinect, <https://dev.windows.com/en-us/kinect>, Nov. 2017.

[28] C. M. Bishop, *Pattern Recognition and Machine Learning*. Secaucus, NJ, USA: Springer-Verlag New York, Inc., 2006.

[29] N. Lazaros, G. C. Sirakoulis, and A. Gasteratos, "Review of stereo vision algorithms: from software to hardware," *International Journal of Optomechatronics*, vol. 2, no. 4, pp. 435–462, Nov. 2008.

[30] J. Pailhous and M. Bonnard, "Steady-state fluctuations of human walking," *Behavioural brain research*, vol. 47, no. 2, pp. 181–189, 1992.

[31] J. Gu, Z. Wang, J. Kuen, L. Ma, A. Shahroudy, B. Shuai, T. Liu, X. Wang, G. Wang, J. Cai, and T. Chen, "Recent advances in convolutional neural networks," *Pattern Recognition*, Oct. 2017.

[32] S. Hochreiter and J. Schmidhuber, "Long Short-Term Memory," *Neural Comput.*, vol. 9, no. 8, pp. 1735–1780, Nov. 1997.

[33] F. Cheng and H. Shen, "An improved recurrent neural network for radio propagation loss prediction," in *Proc. IEEE ICICTA*, vol. 1, Changsha, China, May 2010, pp. 579–582.

[34] J. Zhang and I. Marsic, "Link quality and signal-to-noise ratio in 802.11 WLAN with fading: A time-series analysis," in *Proc. IEEE VTC 2006-Fall*, Montreal, Quebec, Canada, Sep. 2006, pp. 1–5.

[35] J. Donahue, L. Anne Hendricks, S. Guadarrama, M. Rohrbach, S. Venugopalan, K. Saenko, and T. Darrell, "Long-term recurrent convolutional networks for visual recognition and description," in *Proc. IEEE CVPR*, Boston, Massachusetts, USA, Jun. 2015, pp. 2625–2634.

[36] X. Shi, Z. Chen, H. Wang, D. Yeung, W. Wong, and W. Woo, "Convolutional LSTM network: A machine learning approach for precipitation nowcasting," in *Proc. NIPS*. Montreal, Canada: Curran Associates, Inc., Dec. 2015, pp. 802–810.

[37] L. Breiman, "Random forests," *Machine Learning*, vol. 45, no. 1, pp. 5–32, Oct. 2001.

[38] J. Shotton, A. Fitzgibbon, M. Cook, T. Sharp, M. Finocchio, R. Moore, A. Kipman, and A. Blake, "Real-time human pose recognition in parts from single depth images," in *Proc. IEEE CVPR*, Colorado Springs, USA, Jun. 2011, pp. 1297–1304.

[39] L. Breiman, "Bagging predictors," *Machine Learning*, vol. 24, no. 2, pp. 123–140, Aug. 1996.

[40] S. Ioffe and C. Szegedy, "Batch normalization: Accelerating deep network training by reducing internal covariate shift," in *Proc. ICML*, vol. 37, Lille, France, Jul. 2015, pp. 448–456.

[41] I. Sutskever, J. Martens, G. Dahl, and G. Hinton, "On the importance of initialization and momentum in deep learning," in *Proc. ICML*, Atlanta, USA, Jun. 2013, pp. 1139–1147.

[42] Keras, <https://keras.io/>, Nov. 2017.

[43] TensorFlow, <https://www.tensorflow.org/>, Nov. 2017.

[44] F. Pedregosa, G. Varoquaux, A. Gramfort, V. Michel, B. Thirion, O. Grisel, M. Blondel, P. Prettenhofer, R. Weiss, V. Dubourg *et al.*, "Scikit-learn: Machine learning in python," *J. Machine Learning Research*, vol. 12, pp. 2825–2830, Oct. 2011.

[45] T. Wang, M. Umehira, H. Otsu, S. Takeda, T. Miyajima, and K. Kagoshima, "A twin cylinder model for moving human body shadowing in 60GHz WLAN," in *Proc. IEEE APCC 2015*, Kyoto, Japan, Oct. 2015, pp. 188–192.

[46] V. Vukadinović, Ólafur Ragnar Helgason, and G. Karlsson, "An analytical model for pedestrian content distribution in a grid of streets," *Mathematical and Computer Modellinga*, vol. 57, no. 11, pp. 2933–2944, Jun. 2013.

[47] C. Gustafson and F. Tufvesson, "Characterization of 60 GHz shadowing by human bodies and simple phantoms," in *Proc. IEEE EUCAP*, Prague, Czech Republic, Mar. 2012, pp. 473–477.

[48] Kozo Keikaku Engineering, Inc., "Raplab," <http://www4.kke.co.jp/raplab/>, Nov. 2017.

[49] Blender, <https://www.blender.org/>, Nov. 2017.

[50] A. Maltsev *et al.*, "Channel models for 60 GHz WLAN systems, doc.: IEEE 802.11-09/0334r8," *IEEE 802.11 document 09/0334r8*, 2010.

[51] Y. Koda, K. Yamamoto, T. Nishio, and M. Morikura, "Time series measurement of IEEE 802.11ad signal power involving human blockage with HMM-based state estimation," in *Proc. IEEE VTC2017-Fall*, Toronto, Canada, Sep. 2017, pp. 1–5.



**Hironao Okamoto** received the B.E. degree in electrical and electronic engineering from Kyoto University in 2016. He is currently studying toward the M.I. degree at the Graduate School of Informatics, Kyoto University. He is a student member of the IEEE.



and TCP, and QoS and a member of the IEEE.

**Takayuki Nishio** received the B.E. degree in Electrical and Electronic Engineering from Kyoto University in 2010. He received the M.I. and Ph.D. degrees in Communications and Computer Engineering, Graduate School of Informatics from Kyoto University, Kyoto, Japan, in 2012 and 2013, respectively. He is currently an Assistant Professor in Communications and Computer Engineering, Graduate School of Informatics, Kyoto University. His current research interests include communication system design, protocol design particularly MAC resource management in wireless networks. He is



**Kota Nakashima** He is currently studying toward the B.E. degree at the Faculty of Engineering, Kyoto University.



**Yusuke Koda** received the B.E. degree in electrical and electronic engineering from Kyoto University in 2016. He is currently studying toward the M.I. degree at the Graduate School of Informatics, Kyoto University. He is a student member of the IEEE.



**Masahiro Morikura** received his B.E., M.E., and Ph.D. degrees in electronics engineering from Kyoto University, Kyoto, Japan in 1979, 1981 and 1991, respectively. He joined NTT in 1981, where he was engaged in the research and development of TDMA equipment for satellite communications. From 1988 to 1989, he was with the Communications Research Centre, Canada, as a guest scientist. From 1997 to 2002, he was active in the standardization of the IEEE 802.11a based wireless LAN. His current research interests include WLANs and M2M wireless

systems. He received the Paper Award and the Achievement Award from IEICE in 2000 and 2006, respectively. He also received the Education, Culture, Sports, Science and Technology Minister Award in 2007 and Maejima Award in 2008, and the Medal of Honor with Purple Ribbon from Japan's Cabinet Office in 2015. Dr. Morikura is now a professor in the Graduate School of Informatics, Kyoto University. He is a member of the IEEE.



**Yusuke Asai** received the B.E., M.E. and Ph.D. degrees in Nagoya University, Japan, in 1997, 1999 and 2017, respectively. In 1999, he joined Nippon Telegraph and Telephone Corporation (NTT), in Japan. He has been engaged in the research and development of signal processing and resource management techniques for broadband wireless LAN systems. He has served as one of the co-chairpersons of the coexistence ad-hoc group of Task Group ac in IEEE 802.11 Working Group. He is currently a senior research engineer in NTT Network Innovation Laboratories. He received the Young Researcher's Award of the Institute of Electronics, Information and Communication Engineers (IEICE) Japan in 2004 and the Certification of Appreciation for outstanding contributions to the development of IEEE 802.11ac-2013 from the IEEE-SA in 2014. He is a member of IEEE.



**Koji Yamamoto** received the B.E. degree in electrical and electronic engineering from Kyoto University in 2002, and the M.E. and Ph.D. degrees in informatics from Kyoto University in 2004 and 2005, respectively. From 2004 to 2005, he was a research fellow of the Japan Society for the Promotion of Science (JSPS). Since 2005, he has been with the Graduate School of Informatics, Kyoto University, where he is currently an associate professor. From 2008 to 2009, he was a visiting researcher at Wireless@KTH, Royal Institute of Technology (KTH) in

Sweden. His research interests include applications of game theory, spectrum sharing, and in-band full-duplex communications. He received the PIMRC 2004 Best Student Paper Award in 2004, the Ericsson Young Scientist Award in 2006, the Young Researcher's Award and the Paper Award from the IEICE of Japan in 2008 and 2011, respectively, and IEEE Kansai Section GOLD Award in 2012. He is a member of the IEEE.



**Ryo Miyatake** received the B.E., M.E. degrees in University of Electro-Communications, Japan, in 2011 and 2013, respectively. In 2013, he joined Nippon Telegraph and Telephone Corporation (NTT), in Japan. He has been engaged in the research and development of signal processing techniques for wireless communication systems. He is currently a research engineer in NTT Network Innovation Laboratories.